Food and Chemical Toxicology 131 (2019) 110562

Contents lists available at ScienceDirect

Food and Chemical Toxicology

journal homepage: www.elsevier.com/locate/foodchemtox

Anti-diabetic effect of oligosaccharides from seaweed *Sargassum confusum* via JNK-IRS1/PI3K signalling pathways and regulation of gut microbiota

Cheng-feng Yang[a,c,1], Shan-shan Lai[a,d,1], Yi-han Chen[a], Dan Liu[a], Bin Liu[a], Chao Ai[d], Xu-zhi Wan[a], Lu-ying Gao[e], Xin-hua Chen[b], Chao Zhao[a,b,f,*]

[a] College of Food Science, Fujian Agriculture and Forestry University, Fuzhou, 350002, China
[b] Key Laboratory of Marine Biotechnology of Fujian Province, Institute of Oceanology, Fujian Agriculture and Forestry University, Fuzhou, 350002, PR China
[c] College of Food Science and Nutritional Engineering, China Agricultural University, Beijing, 100083, China
[d] School of Food Science and Engineering, South China University of Technology, Guangzhou, 510641, China
[e] Department of Pediatrics, Nanjing First Hospital, Nanjing Medical University, Nanjing, 210006, China
[f] Institute of Chinese Medical Sciences, State Key Laboratory of Quality Control in Chinese Medicine, University of Macau, Taipa, Macau, China

ARTICLE INFO

Keywords:
Sargassum confusum oligosaccharide
Antidiabetic
Insulin signaling pathway
Gut microbiota
High-throughput sequencing

ABSTRACT

Brown seaweed *Sargassum confusum* (C. Agardh) has been used in traditional Chinese medicine to treat a variety of diseases. The aim of the present study was to evaluate the anti-diabetic effect of oligosaccharides from brown seaweed *S. confusum* (SCO). The anti-diabetic effect of SCO was evaluated *in vivo* using high-fat/high-sucrose fed hamsters. Molecular mechanisms of modulating gene expression of specific members of insulin signaling pathways were determined. The components of the intestinal microflora in diabetic animals were also analyzed by high-throughput 16S rRNA gene sequencing. And it was found that SCO had a sequence of sulfated anhydrogalactose and methyl sulfated galactoside units. Fasting blood glucose levels were significantly decreased after SCO administration. Histology showed that SCO could protect the cellular architecture of the liver. SCO could also significantly increase the relative abundance of *Lactobacillus* and *Clostridium* XIVa and decrease that of *Allobaculum*, *Bacteroides* and *Clostridium* IV. The active role of SCO in anti-diabetic effect was revealed by its regulation of insulin receptor substrate 1/phosphatidylinositol 3-kinase and c-Jun N-terminal kinase pathways. These results suggested that SCO might be used as a functional material to regulate gut microbiota in obese and diabetic individuals.

1. Introduction

The number of people suffering from glucose and lipid metabolic disorders has increased exponentially in recent decades. And it has become a major public health problems worldwide (Morgen and Sørensen, 2014). Glucose and lipid metabolic disorders induced by the altered metabolic, hormonal, and immune balances are the common pathological basis and clinical manifestation of type 2 diabetes mellitus (T2DM). Fasting and postprandial high blood glucose and relative insulin deficiency are the key characteristics of T2DM (Garcíajiménez et al., 2016). Obesity is one of the strongest risk factors for the development of T2DM and contributes to approximately 55% of type 2 diabetes cases (Li et al., 2012). Moreover, obesity can be generally associated with insulin resistance (IR), increased oxidative stress, and enhanced inflammatory marker expression (Mohammed et al., 2016). Additionally, IR as a significant pathogenic factor in T2DM also leads to obesity (Chakrabarti et al., 2002). Discovery and development of the novel drugs controlling energy balance will provide the potential tools to fight against T2DM.

Gut microbiota has been regarded as an important part of a dynamic ecosystem in the body, and its composition is influenced by environmental and host factors (He et al., 2015). Gut microbiota is increasingly considered to play a vital role in the development of metabolic disorders. Numerous important studies have shown that the composition and function of gut microbiota serve as environmental factors in the development of T2DM and obesity (Holmes, 2015). Diet has been reported to play a principle role in forming and changing the bacterial community composition of human gut. There are approximately 10^{14} bacteria belonging to more than 1000 phylotypes harboured in human gut. Although the composition of human gut microbiota shows great

* Corresponding author.College of Food Science, Fujian Agriculture and Forestry University, Fuzhou, 350002, China.
E-mail address: zhchao@live.cn (C. Zhao).
[1] Cheng-feng Yang and Shan-shan Lai contributed equally to this research as co-first authors.

https://doi.org/10.1016/j.fct.2019.110562
Received 13 April 2019; Received in revised form 5 June 2019; Accepted 6 June 2019
Available online 07 June 2019
0278-6915/

variation among individuals, most bacteria belong to six well-known bacterial divisions/phyla: Firmicutes, Bacteroidetes, Proteobacteria, Actinobacteria, Fusobacteria, and Verrucomicrobia (Zhao et al., 2019). Obesity is associated with the shift in relative abundance of the two above mentioned dominant bacterial phyla. Specifically, a larger proportion of Firmicutes and relatively lower abundance of the phylum Bacteroidetes were observed in obese individuals (Murphy et al., 2010). Targeting gut microbiota may be promising as a possible therapy for metabolic disorders. High-throughput sequencing technology possesses the more obvious advantages for the study of microbial structure (Li et al., 2010).

Marine algae are rich in bioactive ingredients with diverse biological activities and potential health benefits (Zhao et al., 2018). Marine macroalgal polysaccharides and oligosaccharide derivatives with the prebiotic potential have various effects on animal health, including the modulation of gut microbiota. Multiple kinds of marine algae derived-carbohydrates can be fermented by gut symbionts, which have various effects on intestinal ecology (Shang et al., 2017). The *Sargassum*, a genus of brown seaweed (*Phaeophyceae*) in the *Sargassaceae* family, is a rich source of health-maintaining and promoting agents, such as polysaccharides and polyphenols. A wide range of pharmacological properties of *Sargassum* extracts or isolated components have been recognized, including anticancer, antibacterial, anti-viral, anti-inflammatory, antioxidant, hypoglycaemic, hypolipidaemic, hepatoprotective, and neuroprotective activities (Liu et al., 2012). *Sargassum confusum* (C. Agardh), one kind of *Phaeophyceae*, has been used in traditional Chinese medicine to treat a variety of diseases. The use of functional oligosaccharides improves the balance of the intestinal microflora and reduces the risk of lifestyle-related diseases, such as cardiovascular diseases, obesity and T2DM (Zhao et al., 2017). However, in most cases, there is little available information about the effect of oligosaccharides from *S. confusum* (SCO) on diabetes and gut microflora is available. In our study, the hamsters fed with high-fat/high-sucrose diet (HFSD) were used to construct as a diabetic model. The anti-diabetic activity of SCO was studied *in vivo* and *in vitro* using HFSD-fed hamsters and human hepatoma (HepG2) cells, respectively.

2. Materials and methods

2.1. Preparation and purification of S. confusum oligosaccharide

The air-dried *S. confusum* (Fig. S1) was kindly provided by Qingdao Lanbao Marine Bio-technology Co., Ltd. (Qingdao, China) and identified by Fujian Province Key Laboratory for the Development of Bioactive Material from Marine Algae (Quanzhou, China). One hundred grams of powder were extracted with distilled water (3000 mL) in three cycles in a water bath at 90 °C for 2 h. The combined aqueous extract was centrifuged at 4500 × *g* for 20 min to collect the supernatant. The supernatant was then further concentrated to one-fourth of the original volume using a rotary evaporator at 55 °C under vacuum. The concentrate was precipitated in overnight by adding four volumes of 95% ethanol (v/v) at 4 °C. After centrifugation, the separated polysaccharides extracted from *S. confusum* were collected and then vacuum-dried for further studies using a rotary vacuum evaporator. Polysaccharides were extracted with Sevag reagent to remove proteins, decolourized by macroporous resin AB-8, and degraded by enzymatic hydrolysis to prepare SCO. Then, polysaccharides were dissolved in distilled water at a concentration of 10% (w/v) in which α-amylase, cellulose, pectinase and xylanase were added with the ration of 1:1:1:1 (w/w/w/w). The reaction solution after incubated at 51 °C and pH 6.2 for 3.9 h was mixed with equal volume of 95% ethanol (v/v) to terminate the process of enzymatic hydrolysis. Subsequently, the hydrolysis solution was centrifuged at 4500 × *g* for 15 min to remove the pellet. The target polysaccharide hydrolysates were separated from the supernatant fluid by ultrafiltration membrane with the molecular weight cut-off of 3000 Da. The filtrates were lyophilized and stored at −20 °C. The oligosaccharides were concentrated, passed through a BioGel P-2 gel-filtration column, and then eluted with water to obtain purified SCO product.

2.2. Characterization of SCO by electrospray ionization massspectrometry (ESI-MS), fourier-transformed infrared spectroscopy (FT-IR) and nuclear magnetic resonance (NMR)

The monosaccharide composition of SCO was determined by an Agilent Technologies 7980 gas chromatograph (Agilent, Santa Clara, US) coupled with a flame ionization detector and DB-170 column (30 m × 0.32 mm × 0.25 μm). Briefly, 10 mg of SCO was hydrolysed into monosaccharides by 3.0 mL of 2.0 mol/L trifluoroacetic acid at 105 °C for 9 h, then the hydrolysate and monosaccharides, containing standard sugars (arabinose, fucose, glucose, mannose, rhamnose, and xylose), were derivatised by hydroxylamine hydrochloride and pyridine. Finally, the derivatives of hydrolysate and monosaccharides were analysed by gas chromatography. Negative-ion ESI-MS was performed on Agilent Q-TOF 6520 instrument (Agilent, Santa Clara, US) for the sulfated oligosaccharide. The *m/z* range was acquired from 100 to 1000 Da. The conditions used for the ESI source were as follows: capillary voltage of 3500 V, drying gas temperature of 350 °C, atomizing gas pressure of 35 psi, and dry gas flow rate of 8 L/min. Fourier transform infrared spectra of SCO were recorded in the wavelength range of 4000–400 cm^{-1} using an Impact 410 Nicolet FT-IR spectrometer (Thermo Co., Madison, WI, USA) and KBr disc method to prepare the specimen. Lyophilized samples were exchanged thrice with 99.9% atom D_2O. One-dimensional 600 MHz ^1H and ^{13}C NMR spectra were recorded on a Bruker ADVANCE III HD 850 MHz spectrometer (Brucker, Bruker BioSpin GmbH, Germany) at 25 °C. The relaxation delay, acquisition time, and number of transients for 1D ^1H NMR spectra acquired were set at 1 s, 1.9268 s, and 16, respectively. The spectrum width was 17006.8 Hz, resulting in a spectral size of 65536 data points. The 1D^{13}C NMR spectrum was recorded with a relaxation delay of 2 s, an acquisition time of 0.6423 s, a spectrum width of 51020.4 Hz, and a transient number of 256. The receiver gain was set to 10 and 2050 for 1D ^1H and 1D^{13}C NMR, respectively. Two-dimensional ^1H–^1H correlation spectroscopy (COSY) and ^1H–^{13}C heteronuclear single-quantum coherence spectroscopy (HSQC) were performed following the standard procedures of the Bruker Company and measured at 25 °C. In 2D COSY and HSQC NMR experiment, 2 and 4 transients were accumulated per t_1 increment, the acquisition time was set to 0.1204 and 0.06 s, the receiver gain was set to 2050 and 1440, respectively. A relaxation delay of 1.5 s was used for COSY and HSQC experiments. Spectra were processed with MestReNova 8.0 software (Mestrelabs Research SL, Santiago de Compostella, Spain).

2.3. Animals, diabetes induction and experimental design

Healthy male Syrian golden hamsters (specific-pathogen-free, 8 weeks old; 100 ± 10 g) were used in this study. Animals were fed a standard chow diet (No.1022, Huafukang Bioscience Co. INC., Beijing, China; Table S2) and water *ad libitum*, and maintained in hygienic environment (temperature 27 ± 1 °C; 60 ± 10% humidity; and a 12 h/12 h light/dark cycle) in sterile polypropylene cages. All experimental procedures were strictly in accordance with the Guide for the Care and Use of Laboratory Animals published by the US National Institutes of Health (NIH Publication No. 85–23, revised 1996). The ethical review board of Fuzhou General Hospital of Nanjing Military Command provided ethical approval (27/03/2016 & FZZY-2016) of animal use protocol. Adequate measures were taken to minimize pain of experimental animals. As a normal group, eight male hamsters were fed basic chow. Other 16 hamsters fed with high-fat/high-sucrose diet (HFSD, containing 1% cholesterol, 1% NaCl, 10% lard, 10% yolk powder, 10% sucrose, 0.5% bile salt, and 67.5% standard chow) were randomly divided into two groups: a model and an SCO-treated group. Animals in

the normal and model groups were treated with saline by intragastric administration, and those in the SCO-treated group were simultaneously gavaged with 150 mg/kg body weight of SCO solution (30 mg/mL) once daily. On the 60th day of the experiment, the faeces of hamsters in each group were collected and placed in a dry sterile tube, then immediately placed stored at −80 °C.

2.4. Determination of hypoglycaemic activity of SCO

The fasting blood glucose (FBG) and body weight were synchronously measured once a month after a 12-h fast. FBG levels were detected by OMRON Active Glucose Monitor (Kyoto, Japan). Fasting serum insulin (FSI) was measured by hamster insulin ELISA kit from Shanghai MLBIO Biotechnology Co. Lit (Shanghai, China). After two months of continuous intragastric administration, all hamsters were fasted for 12 h with free access to water for oral glucose tolerance test (OGTT). Hamsters were administered with 2 g/kg glucose by gavage, then, blood samples were collected and tested using glucose meter at 0, 0.5 and 2 h after glucose administration. The area under curve (AUC) value was calculated as follow: $AUC = 0.5 (G_{0\ h} + G_{0.5\,h}) \times 0.5 + 0.5 (G_{2\ h} + G_{0.5\,h}) \times 1.5$. All analyses were performed according to the protocols provided by the manufacturers.

2.5. Determination of the serum biochemical indices

Hamsters were anaesthetized mildly with ether anaesthesia after fast for 12 h with free access to water, and blood samples were collected by puncturing the retro-orbital sinus with a 10 μL capillary tube. A 200-μL aliquot of blood sample was stabilized in EDTA-coated tubes. Serum was separated by centrifugation at 1000 rpm for 10 min. The alanine transaminase (ALT), aspartate transaminase (AST), total cholesterol (TC), triglyceride (TG), high-density lipoprotein (HDL) and low-density lipoprotein (LDL) were detected on AU480 automatic biochemical analyser (Beckman Coulter, Inc., USA).

2.6. Histopathological analysis

All animals were euthanized by intraperitoneal injection of 7% chloral hydrate (0.5 mL/100 g body weight) and anatomized after fixation. The liver was excised and washed with ice-cold 0.9% of saline solution, then fixed in 10% formalin. Histopathological analysis of the liver was conducted by cutting 2-mm sections of the tissues using a microtome, embedding in paraffin and staining with haematoxylin and eosin (H&E).

2.7. Dynamic profile of intestinal microflora in response to SCO

The fecal bacterial DNA of each sample was extracted using E.Z.N.A.® Stool DNA Kit (Omega, Norcross, USA) in accordance with the manufacturer's instructions. The V3–V4 hypervariable domain of 16S rRNA gene was PCR amplified from microbial genome DNA. The primers pairs (Forward: 5′-CCCTACACGACGCTCTTCCGATCTGCCTACGGGNGGCWGCAG-3′ and Reverse: 5′-GACTGGAGTTCCTTGGCACCCGAGAATTCCAGACTACHVGGGTATCTAATCC-3′) were designed. PCR reactions contained 10–20 ng of DNA template, 2 × Taq master Mix (Thermo Scientific, Waltham, MA, USA), 10 μM primers, and H_2O. The following thermal cycling conditions were used: initial denaturation at 94 °C for 3 min; 5 cycles at 94 °C for 30 s, 45 °C for 20 s, and 60 °C for 30 s; 20 cycles at 94 °C for 30 s, 55 °C for 20 s, and 72 °C for 30 s; and a final extension at 72 °C for 5 min. PCR amplification products were purified using the Agencourt AMPure XP kit (Beckman, CA, USA) and quantified using the Qubit dsDNA HS Assay Kit (Invitrogen, Grand Island, NY, USA). Purified libraries were sent for sequencing on the Illumina Miseq™ platform (Sangon Biotech, Shanghai, China). The bacterial sequence reads were aligned to the known 16S rRNA genes of a reference database acquired from the Ribosomal Database Project (RDP). The RDP classifiers were utilized to taxonomically assign bacterial sequences. Based on the phylogenetic relationship between representative readings (*i.e.,* operational taxonomic units, OTUs) from different samples, FastUniFrac was used to analyse the structures of microbial community in different samples.

2.8. RNA extraction and real-time PCR

The insulin-resistant human hepatoma (IR-HepG2) cells for the determination of glucose consumption were prepared by our reported procedure (Yang et al., 2017). The IR-HepG2 cells were induced by 2 μmol/L of dexamethasone for 72 h from HepG2 cells (purchased from the Cell Bank of Chinese Academy of Sciences, Cat.No. TCHu 72). For RNA extraction, IR-HepG2 cells were treated with medium or medium with 200 μg/mL of SCO for 24 h. The cells were collected and washed three times with ice-cold phosphate buffer solution (PBS, pH 7.0). The total cellular RNA was extracted using Trizol reagent (Invitrogen, NY, USA) and reverse-transcribed into first-stand cDNA using cDNA synthesis kit (Takara, Dalian, China). RT-PCR of GAPDH, insulin receptor substrate 1 (IRS1), c-Jun N-terminal kinase 1 and 2 (JNK1/2), phosphatidylinositol 3-kinase (PI3K), and glucose transporter type 4 (GLUT4) were performed using SYBR Green RT-PCR kit (Invitrogen, NY, USA) and the specific primers as follows: GAPDH, F: 5′-TGGGTG TGAACCATGAGAAGT-3′, R: 5′-TGAGTCCTTCCACGATACCAA-3’; IRS1, F: 5′-GTCAGTCTGTCGTCCAGTAGCA-3′, R: 5′-GAACCAGACACCGAAG CACTA-3’; JNK1, F: 5′-ATCCATCATCATCGTCGTCTG-3′, R: 5′-ACTCC CCATCCCTCCCAC-3’; JNK2, F: 5′-CAAGGGATTGTTTGTGCTGC -3′, R: 5′-TGGTTCTGAAAAGGACGGCT-3’; PI3K, F: 5′-CAGTAGGCAACCGTG AAGAAA-3′, R: 5′-GGTGAAGATTCTACATTTGGAGG-3’; and GLUT4, F: 5′-CCCATTCCTTGGTTCATCG-3′, R: 5′-CATAGCCTCCGCAACATACTG-3’. Amplifications were performed under the following thermal cycling conditions: 95 °C for 3 min, 45 cycles at 95 °C for 7 s, 57 °C for 10 s, and 72 °C for 15 s. An ABI StepOne Plus Real-Time PCR system (Applied Biosystems, USA) was used to analyse the quantity of the mRNA, which was normalized to that of GAPDH.

2.9. Western blot analysis

The treated HepG2 cells were collected and washed as described above, then solubilized by lysis buffer on ice for 30 min. BCA protein assay kit (Beyotime, Shanghai, China) was used to determine concentrations of lysate protein. A combined lysis protein in 5 × loading buffer was denatured for 5 min at 100 °C. A 15-μL aliquot of molecular weight markers (15–130 kDa, Sangon Biotech, Shanghai, China) and protein samples were subjected to SDS-PAGE, then transferred to a polyvinylidene difluoride (PVDF) membrane. The PVDF membrane was blocked in the Western BLoT Blocking Buffer (Protein Free) (Code No. T7132A, Takara, Dalian, China) at room temperature for 1 h, followed by incubated with anti-GAPDH (0.5 μg/mL), anti-IRS1 (1 μg/mL), anti-JNK1/2 (10 μg/mL), anti-PI3K (1 μg/mL), or anti-GLUT4 (1 μg/mL) rabbit polyclonal antibodies (Abcam, Cambridge, UK), respectively, at 37 °C for 1 h. After incubation with primary antibodies, the blotting membrane was washed four times with 1 × TBST once every 10 min. The membrane was further incubated with alkaline phosphatase-conjugated goat anti-rabbit IgG (H + L) (1 μg/mL) mixed in blocking buffer at 37 °C for 1 h and washed according to the above-described procedure. The protein blots were visualized using BCIP/NBT Alkaline Phosphatase Color Development Kit (Beyotime, Shanghai, China) and quantified using GeneTools from Syngene software.

2.10. Potential network from SCO intake to antidiabetic effect

The correlation between SCO, intestinal microflora, physiological indexes and relative genera in pathways were calculated by Spearman's rank correlation coefficient and visualized by network using Cytoscape (Version 3.2.1).

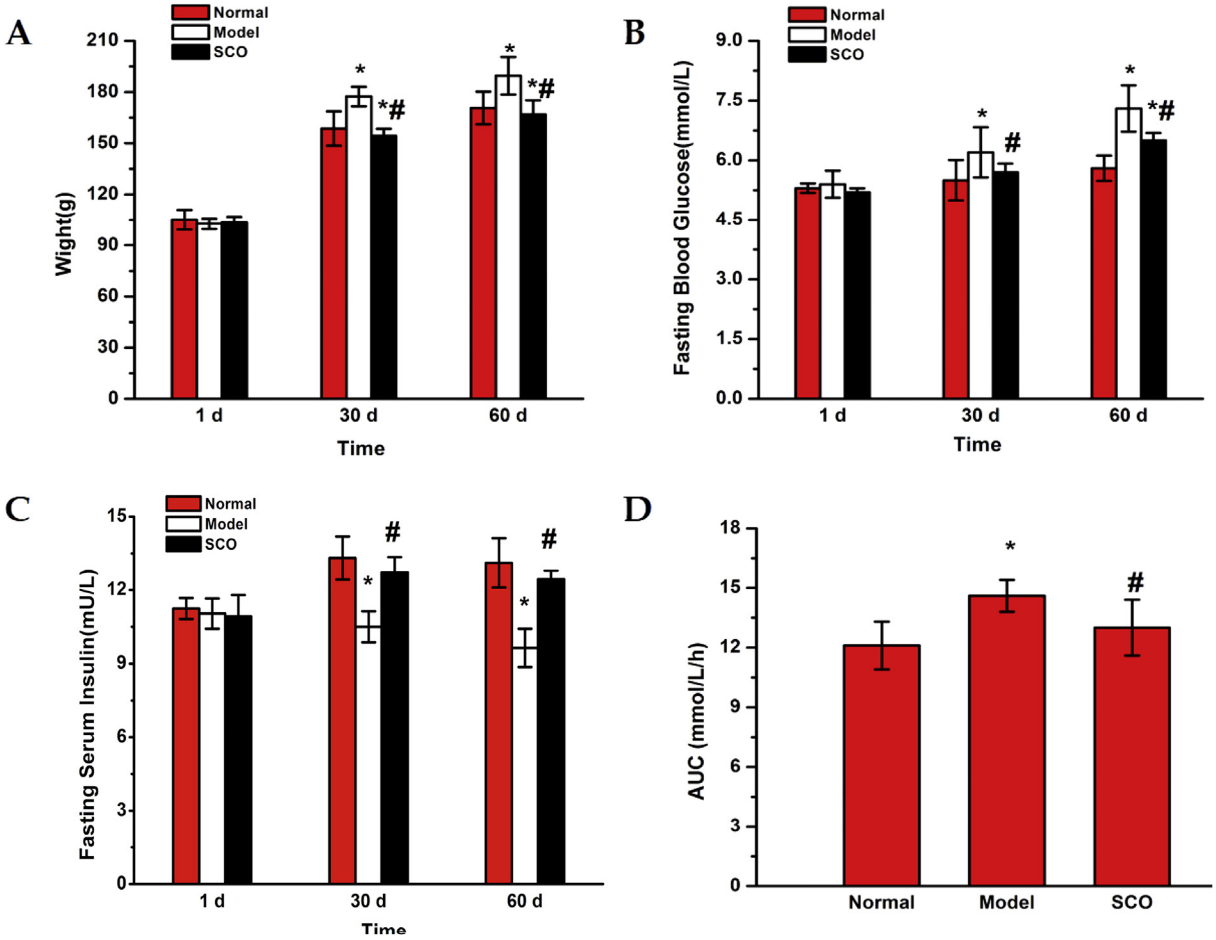

Fig. 1. Effects of SCO on body weight (A), fasting blood glucose (B), serum insulin (C), and AUC (D) levels on *in vivo* high-fat/high-sucrose fed hamsters. Values are expressed as mean ± SD (n = 8). $^{*}p < 0.05$, compared with normal group; $^{\#}p < 0.05$, compared with model group.

2.11. Statistical analysis

All values were expressed as the mean ± SD. Statistical significance was determined using analysis of variance (ANOVA) followed by Dunnett's test. A *p*-value less than 0.05 was considered statistically significant differences.

3. Results

3.1. Characterization of novel oligosaccharide from S. confusum

The hydrolytic SCO was purified using BioGel-P2 chromatography, and its origin from the specific SCO was confirmed by MS analysis. The monosaccharide Gal was detected with gas chromatography analysis. The results showed that SCO was composed of fucose, arabinose, xylose and glucose (Fig. S2). The FT-IR spectra obtained from SCO displayed peaks between 4000 cm^{-1} and 400 cm^{-1} (Fig. S3A). The absorption peak between 800 cm^{-1} and 400 cm^{-1} generally corresponded to C–O–C and C–O–H bond vibrations. Galactopyranose residues were represented by the absorption band at 843 cm^{-1}. The carboxyl or glucuronic acid peak occurred at approximately 1420-1300 cm^{-1}. SCO contained carbonyl, carboxyl or glucuronic acid, and galactopyranose residues. In the mass spectrum, monosaccharide D-galactopyranose [Gal] ion with *m/z* 179.04 and its most-abundant 3,6-anhydro (anGal) fragment ion, resulting from the loss of water molecules, with *m/z* 161.03 were observed (Fig. S3B). Therefore, it was concluded that the ion with *m/z* 341.09 indicated a composition of one Gal unit and one anGal unit [Gal-anGal]. In addition, mono-sulfated galactose [$GalSO_3Na$–Na] losing a water molecule was observed at *m/z* 255.23. The fragmentation identity of the ion with *m/z* 404.09 was sulfated galactose [$GalGalSO_3$]. ESI-MS analyses revealed that the ion with *m/z* 483.02 was assigned to a sulfated oligosaccharide [$Gal(SO_3)Gal(SO_3Na)$Me], and its fragment ion from the loss of sodium molecules with *m/z* 461.04 was observed. The partial hydrolyzates of the ion with *m/z* 118.93 and *m/z* 341.09 formed [$Gal(SO_3)Gal(SO_3)$Me]. In addition to the main peak, an intensive ion peak at *m/z* 439.06 corresponded to methyl sulfated galactoside [$Gal(SO_3Na)$Me–Na]. The ESI-MS of [Gal (SO_3Na)Me–Na] was complex and contained one intensive signal (with *m/z* 179.04) from the breakage of glycosidic bonds and the cleavage of a dehydrated sulfated galactose residue. The identified disaccharide was composed of sulfated anhydrogalactose and methyl sulfated galactoside units. The above results demonstrated that SCO was a sulfated oligosaccharide containing one Gal unit and one anGal unit, sulfated galactose, sulfated anhydrogalactose and methyl sulfated galactoside units.

In ^{1}H-NMR spectrum (Fig. S4A), the chemical shifts at 4.2–5.2 ppm signal displayed the characteristics of carbohydrates (Zhao et al., 2016). The anomeric signal between 4.5 and 5.8 ppm except 4.71 ppm corresponding with the α-configuration of the glycan residues ($\delta > 5.00$ ppm) and β-glucose residuals ($\delta < 5.00$ ppm) (Vinogradov and Wasser, 2005). NO aromatic compound signal was observed in the region 6.5–9.5 ppm. The proton chemical shifts from 3.5 to 4.5 ppm indicated the hydrogen atom of glycosidic rings shift from H-2 to H-6 (Cheng and Neiss, 2012). SCO contained the signals from the anomeric proton at 5.13 and 4.54 ppm characteristics of 3,6-α-L-anhydrogalactose and β-D-galactose, respectively (Maciel et al., 2018).

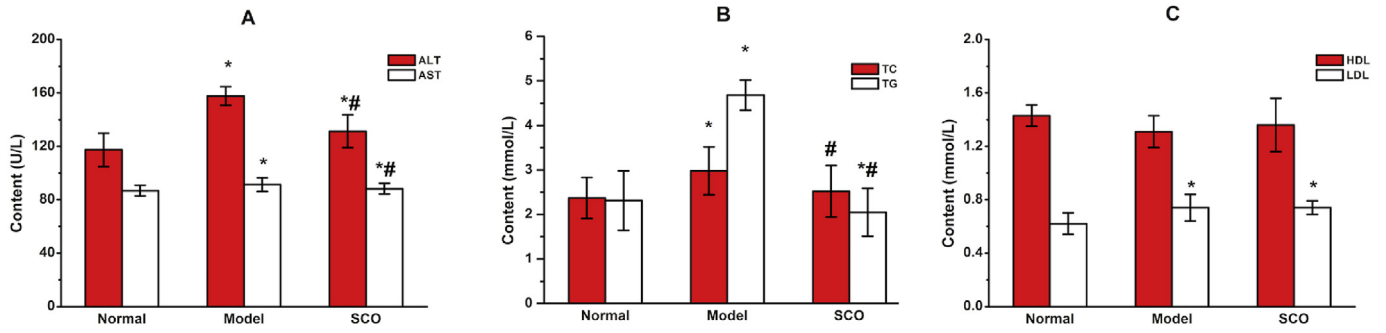

Fig. 2. Effects of SCO on ALT/AST (A), TG/TC (B), and HDL/LDL (C) levels on *in vivo* high-fat/high-sucrose fed hamsters. Values are expressed as mean ± SD (n = 8). $^{*}p < 0.05$, compared with normal group; $^{\#}p < 0.05$, compared with model group.

Signal observed at 4.45 ppm which was attributed to H-1 of β-D-galactose linked to α-L-galactose-6-sulfate. The resolution of signals at 3.40 ppm revealed protons of methyl groups of 6-*O*-methyl-D-galactose (Barros et al., 2013). No signal was observed at 5.34 ppm which was assigned to anomeric proton of 6-*O*-sulfate-L-galactopyranose although sulfated anhydrogalactose had been found as a high intense peak in the LC-MS experiment. In region 90–110 ppm, 7 different anomeric carbons were detected at 102.87, 96.39, 95.85, 95.70,92.24, 92.04 and 91.77 ppm were detected in the ^{13}C-NMR spectrum (Fig. 4SB). Pyranose ring forms of sugar residues were represented by no signal in the region 82–88 ppm. The resonance-absorption peaks of C-2 to C-5 were observed from 70 to 78 ppm. The C-6 for pyranoside resonates occurred from 60 to 64 ppm. The characteristic chemical shifts due to 6-*O*-methyl-D-galactose (73.81 and 71.86 ppm) were also observed (Mazumder et al., 2002). In the ^{1}H–^{1}H COSY NMR spectrum (Fig. S4C), H5/H6 could be observed in δ3.69/1.33 and δ4.16/1.27, which assigned to the fucose or rhamnose. At the same time, C1 to C6 could be assigned through the ^{1}H–^{13}C HSQC NMR spectrum (Fig. S4D). There was cross peak of H1/C1 (δ4.45/96.39) were assigned to the β-D-galactose. The cross peak could be noticed in δ3.50/78.40, which attributed the existence of xylose (Molaei and Jahanbin, 2017).

3.2. Effects of SCO on body weight in diabetic hamsters

The body weight was measured on the 1st, 30th, and 60th days during treatment (Fig. 1A). A steep increase was observed in body weight of all hamsters, and the body weight of the model and HFSD-fed group increased most significantly ($p < 0.05$). Animals in the SCO-treated, HFSD-fed group showed an obviously lower body weight than in the model group after 30 and 60 days of administration ($p < 0.05$). Furthermore, SCO treatment in HFSD-fed hamsters resulted in a significant loss of body weight when compared to normal, basic chow-fed hamsters ($p < 0.05$).

3.3. Effects of SCO on fasting blood glucose and serum insulin levels

The effects of SCO on FBG and FSI levels in diabetic animals on different treatment days were shown in Fig. 1B and C. Initially, there was no significant difference in FBG among the three groups. FBG levels were noticeably elevated in the model group compared with the normal group on the 30th/60th days. Hamsters treated with SCO for 30 days showed lower FBG levels than those in the model group. The crucial step was to determine whether SCO could maintain blood glucose level in normal till the end of the study. It was observed that after 60 days of SCO treatment, the FBG level of hamsters taking SCO was significantly decreased compared with the model group ($p < 0.05$). Furthermore, the FSI level in the model group declined compared with the normal group. SCO slightly increased the FSI level, while there were no statistically significant differences in the SCO-treated group. These results indicated that SCO could help the hamsters fed with HFSD in maintaining the FBG and FSI levels within the normal range.

3.4. Effects of SCO on oral glucose tolerance in diabetic hamsters

Glucose tolerance is regarded as a crucial indicator reflecting the degree of T2DM. The AUC of glucose in different groups was shown in Fig. 1D. The results of OGTT demonstrated a quick increase in blood glucose in the model group after 30 min of glucose administration. The integrated AUC for glucose was significantly higher in the model group than in the normal group ($p < 0.05$), which indicated that HFSD-fed hamsters showed obvious significant impairment in tolerance to exogenously administered glucose. Treatment with SCO for 60 days had a notable significant effect on ameliorating the impaired glucose tolerance ($p < 0.05$).

3.5. Effects of SCO on the serum biochemical values in diabetic hamsters

To determine the SCO ability to maintain the normal blood parameters, the levels of serum lipid and AST and ALT of the hamsters treated with SCO were compared with the normal hamsters to determine the ability of SCO in maintaining the normal blood parameters. The increases of epididymis weight (Fig. S5), ALT, AST, TC, TG and LDL (Fig. 2) indicated that hamsters in the model group were characterized as obesity and hyperlipidaemic. There were no significant differences in HDL levels in all groups. SCO showed the ability to maintain the TC level in blood serum at a nearly normal level even after 60 days of treatment. In addition, the levels of ALT, AST, and TG in SCO group were significantly decreased in comparison with those in the model group ($p < 0.05$). Taken together, these results indicated that the ability of SCO to protect the liver from damage.

3.6. The liver protective effect of SCO in diabetic hamsters

H&E staining of liver sections was conducted to determine the SCO effect on the histopathology of the liver (Fig. 3). Normal architecture of the liver parenchyma was observed in the normal group (Fig. 3A). The histological and pathological observations of the liver showed that a small quantity of the inflammatory cells were accumulated in inflammatory foci in the model group. Local hepatocyte necrosis, congestion and dilation of central vein were also noted in diabetic hamsters (Fig. 3B). By contrast, the inflammatory infiltration and hepatocyte necrosis were more insignificant in the SCO-treated group, which indicated the role of SCO in protecting the liver tissues prone to be damaged when obesity occurred. Moreover, there was extensive hepatocyte vacuolation, indicating fat accumulation in the liver of HFSD-fed hamsters. However, SCO treatment for 60 days efficiently ameliorated lipid accumulation in hepatocytes (Fig. 3C). The liver weight of animals in the SCO group was slightly lower than that in the model group, while there was no statistically significant difference between the two groups (Fig. S5). These results indicated the ability of SCO to protect liver from

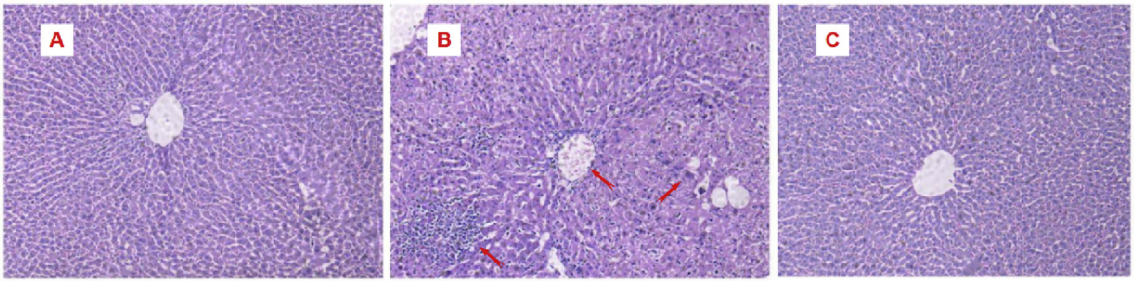

Fig. 3. Effect of SCO on histology of livers from normal (A), model (B) and SCO-treated (C) groups hamsters for 8 weeks (magnification, 10 ×). Arrows from left to right indicate: infiltrating inflammatory cells, congestion and fat accumulation.

inflammation and hepatopathy as well as to maintain the hepatic cells in an almost normal condition.

3.7. Species abundance and structure analysis of gut microflora

A total of 76,037, 25,559 and 74,782 of valid sequences and 1,799, 1,446, and 1797 of OTUs were obtained from gut microflora in the normal, model, and SCO-treated groups, respectively, which indicated high abundance of gut microbiota in hamsters (Table S1). Meanwhile, the coverage index was 0.9925, 0.9798, and 0.9929 in these three groups, respectively, indicating that the sequences were almost detected in the samples. Chao, ACE, and Shannon index are important parameters in the alpha diversity analysis to estimate the diversity of species in ecology. Compared with model hamsters, the SCO administration group showed higher Chao, ACE index and lower Shannon index in faeces, which demonstrated the increased gut bacterial diversity in SCO-fed hamsters.

At the phylum level, *Bacteroidetes*, *Firmicutes*, *Proteobacteria*, and *Actinobacteria* were the dominant bacteria detected among three groups (Fig. 4 and Fig. S6). Comparing the gut microbiota compositions, the *Firmicutes*, *Proteobacteria*, and *Actinobacteria* relative abundances were significantly increased in the faeces of the HFSD-fed hamsters, but the *Bacteroidetes* abundance decreased (Fig. 4B). The composition of gut microbiota in the SCO-treated group (Fig. 4C) was generally similar to that in the normal group (Fig. 4A). The composition of gut microbiota in different groups were divided into two distinct clusters (Fig. S6), which suggested that the bacteria of HFSD-fed hamsters differed significantly from those of the normal and SCO-treated groups, however, there was no obvious difference between the normal and SCO-treated groups. The above results indicated that SCO have the potential to maintain the balance of gut microbiota in HFSD-fed hamsters.

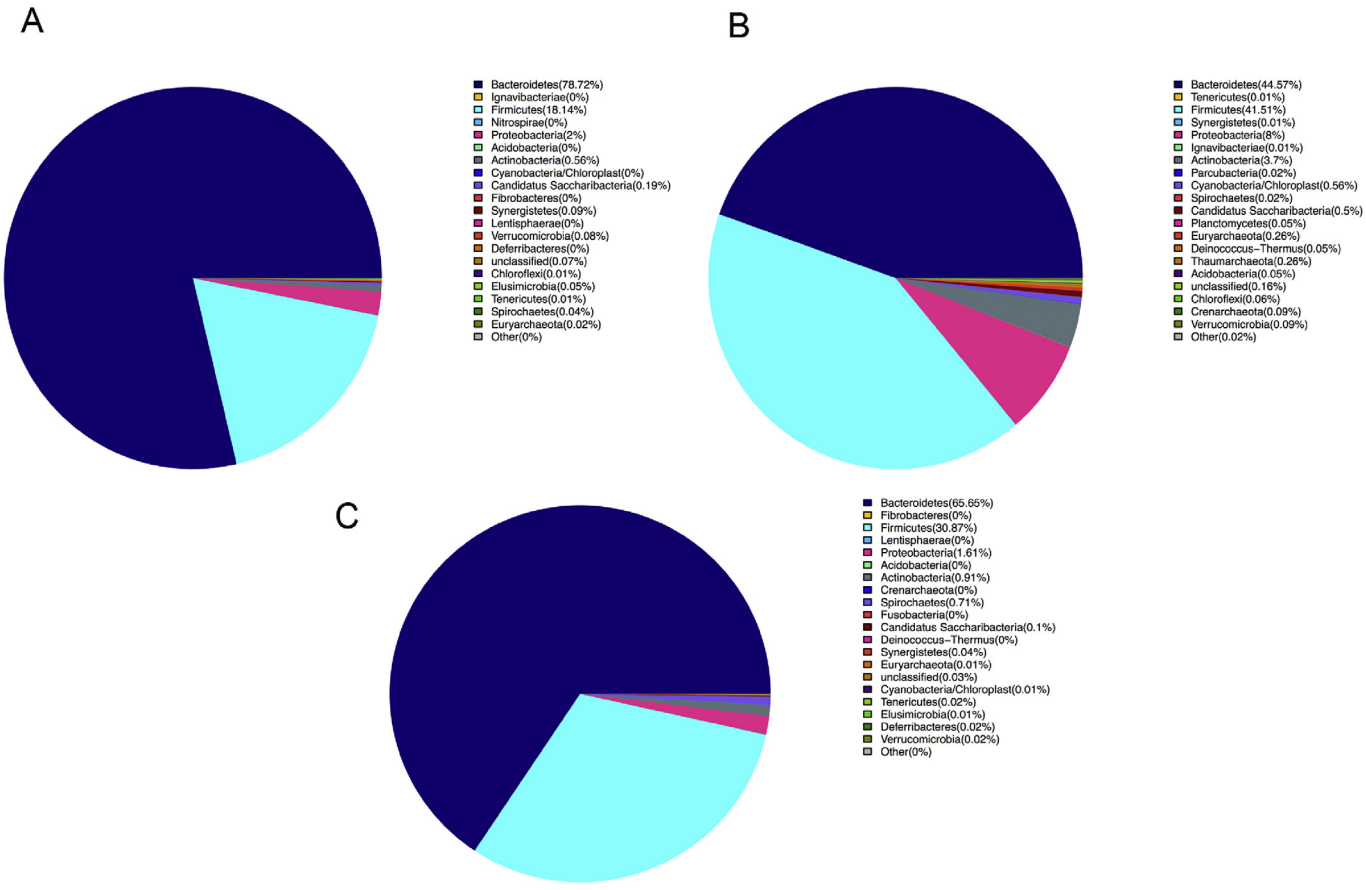

Fig. 4. Relative abundance of bacterial phyla of gut microbiota in normal group (A), model group (B) and SCO-treated group (C).

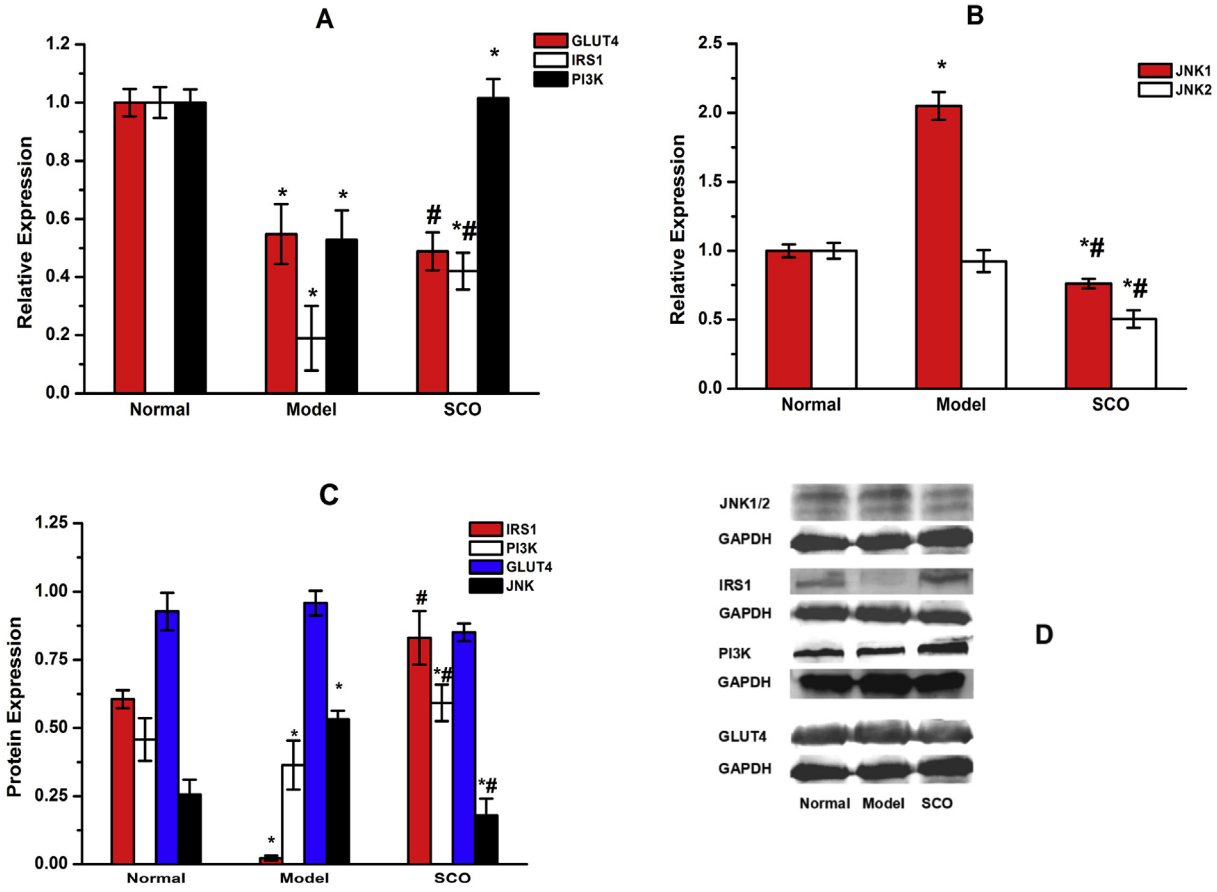

Fig. 5. Effects of SCO treatment on the level of GLUT4, IRS1, PI3K (A), and JNK (B) expression, and protein levels of GLUT4, IRS1, PI3K, and JNK (C), signals were normalized with those of GAPDH; (D) Western blot analysis; JNK1/2 and GLUT4 used the same GAPDH housekeeping gene expression as control. $^{*}p < 0.05$, compared with normal group; $^{\#}p < 0.05$, compared with model group.

3.8. Regulatory action of SCO on gut microbiota in diabetic hamsters

The abundances of *Barnesiella*, *Coprobacter*, *Tannerella*, *Eubacterium*, and *Clostridium XIVa* were significantly higher in the SCO-treated group compared with the model group (Fig. S6). *Lactobacillus* bacteria increased modestly in the gut microbiota of animals treated with SCO, which was consistent with beneficial effects on the prevention and treatment of some disorders. The *Allobaculum*, *Bacteroides*, and *Clostridium* IV were significantly reduced after SCO treatment.

3.9. Effect of SCO on mRNA expression in signalling pathways

There was a significant decrease in the mRNA expression levels of GLUT4, IRS1, and PI3K genes in the diabetic model group when compared with the normal group, as shown in Fig. 5A ($p < 0.05$). SCO treatment could significantly upregulate the expression of IRS1 and PI3K genes, respectively ($p < 0.05$). Moreover, SCO administration significantly reduced the gene expression of JNK1 and JNK2 in the hepatic cells compared with the model group ($p < 0.05$) (Fig. 5B). Above results indicated that SCO might ameliorate hepatic insulin resistance by regulating IRS1/PI3K and JNK signaling pathways.

3.10. Effect of SCO on protein expression in signaling pathways

Western blotting was carried out to analyze the protein expression of GLUT4, IRS1, PI3K, and JNK1/2 were selected for analysis by western blotting (Fig. 5C and D). The concentrations of the protein extracted in the normal, model and SCO groups were 302.61 ± 0.16, 313.60 ± 5.20, and 294.63 ± 5.10 μg/mL, respectively. Protein expression levels of IRS1 and PI3K ($p < 0.05$) were higher in the SCO group than the model group. In contrast, after treatment with SCO, JNK1/2 expression was reduced ($p < 0.05$). These results were equivalent to the findings on mRNA expression indicated that the mechanism of the hypoglycaemic effect induced by oligosaccharide from *S. confusum* might consist in the modification of the hepatic IRS1, PI3K, and JNK1/2 gene and related protein expression.

3.11. Potential network from SCO intake to antidiabetic effect

SCO intake results in the interaction with intestinal microbiome and further elicits host's antidiabetic effect, which altogether were reminiscent of the domino effects. A network was constructed to better explain the causal relationships among SCO, bacterial species, and gene regulation (Fig. 6). The intake of SCO promoted the growth of *Lactobacillus* and *Bifidobacterium*, which were able to stimulate the host's anti-diabetic effect, accompanied by the modification in the gene and protein expression of hepatic IRS1, PI3K, and JNK1/2.

4. Discussion

The main cause of T2DM is obesity-driven hepatic insulin resistance along with inadequate insulin secretion by pancreatic β-cells to offset this resistance (Kusminski et al., 2006). The edible seaweed *Sargassum* is traditionally used to against several human diseases. Motshakeri et al. (2014) have found that ethanolic and aqueous extracts of *S. polycystum* significantly reduced blood glucose by increasing the insulin sensitivity, and reduced the liver damages in type 2 diabetic rats. However, the relationship between its glycan structure and biological activity has not

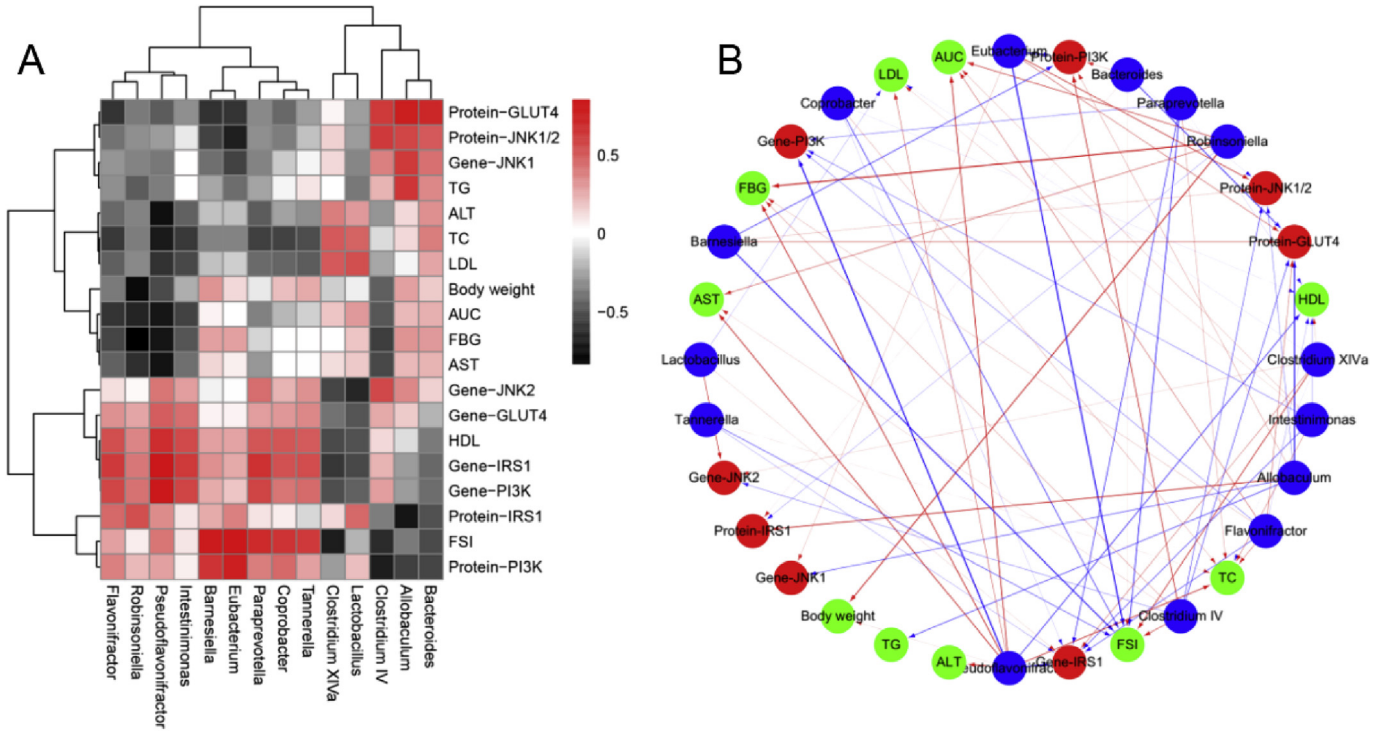

Fig. 6. Heatmap of Spearman's correlation (A) and visualization of the correlation network according to partial correlation (B) between gut microbiota of significant differences and glucose metabolic associated parameters. The intensity of the color represents the degree of association between gut microbiota and glucose metabolic parameters. The blue or red real lines showed the positive or negative correlations, respectively. Gene- or Protein-PI3K, -IRS1, -GLUT4, and -JNK1/2: the modification in the gene and protein level expression of PI3K, IRS1, GLUT4, and JNK1/2, respectively. (For interpretation of the references to colour in this figure legend, the reader is referred to the Web version of this article.)

yet been elucidated due to its complexity, despite many reviews and studies focusing on it. MS with soft desorption/ionization is increasingly becoming an important tool for the analysis of glycan oligosaccharides due to its accuracy, sensitivity, selectivity, and speed (Zhao et al., 2017). Functional oligosaccharides are associated with a variety of biological processes linked to hypoglycaemic and hypolipidaemic activities. Marine oligosaccharides have attracted attention in drug development. Many reports have found numerous potential antidiabetic compounds from *Sargassum* species, in which polyphenols and polysaccharides are the main bioactive substances (Zhao et al., 2018). However, oligosaccharides from *S. confusum* have not been well studied. Above mentioned studies have not reported structural components identical to those in SCO. Therefore, it could be concluded that SCO is a novel oligosaccharide isolated from *S. confusum*. In the present work, the effects of SCO were evaluated in HFSD-fed Syrian golden hamsters. SCO ameliorated the abnormality of blood glucose control and the impaired glucose tolerance in diabetic animals, which may relate to the increased level of insulin which is considered as an important hormone for the regulation of glucose metabolism and for the treatment of diabetes. The higher antidiabetic activity of SCO may be due to its lower molecular weights. Moreover, the noticeably ascendant body weight as well as the increase in ALT, AST, TC, TG, and LDL in model hamsters indicated that the obesity was induced by HFSD. SCO showed the ability to decrease the TC level to an almost normal level after 60 days of treatment. This could be explained by the previous study results, which demonstrated that the blood glucose-lowering action was related to the low TC level (Kumar et al., 2009).

Over the past decade, T2DM and obesity have been associated with inflammation. The accumulated triglycerides lead to the increased size (hypertrophy) of the visceral adipocytes, which further 'spill lipids' into their immediate vicinity, thus initiating a local inflammatory response within adipose tissue resident macrophages (Spyridaki et al., 2016). Anti-inflammatory and antidiabetic effects of brown seaweeds and their extracts have been reported (Han et al., 2015). Fucoidans are capable of interacting with immune system and enhance specific mechanisms of host response (Ferreira et al., 2015). In the present study, SCO effectively reduced the mild inflammation and fat accumulation induced by HFSD in hamster hepatocytes. It may also maintain the normal insulin secretion by reducing inflammation in a long-term HFSD-induced animal model, as previously reported (Oh et al., 2016). The elevated levels of serum AST and ALT levels may be due to some underlying reasons such as toxicity, inflammation, hypoxia, and tissue trauma. They were regarded as the most sensitive and specific indicators measured with a blood test to assess the liver function or liver damage. ALT and AST in the SCO group were significantly lower than in the model group ($p < 0.05$), which further indicated the potential liver protective action of SCO. The above results indicated that SCO could protect hamsters from hepatopathy and maintain the hepatic factors close to normal conditions.

This study was also conducted to determine the effect of SCO on modulating gut microbiota in HFSD-fed Syrian golden hamsters by high-throughput next-generation 16S rRNA gene sequencing. Microbial alterations in the gut are closely related to the composition of faecal microbiota, hence research on the diversity of faecal microbiota helps in deeper understanding of the changes in microbial population. Gut microbiota is increasingly considered as a vital factor in the maintenance of body homeostasis and the development of metabolic disorders, linked to several human diseases, such as diabetes and obesity. Obviously, the diversity of gut microbiota varied after treatment with SCO. The sequencing and OTU number in the model group were significantly lower than those in other two groups, and those in the SCO treatment group were similar to the normal group. Thus, it is indicated that SCO administration significantly influenced the abundance of gut microbiota in hamsters. The composition analysis of gut microbiota indicated that compared with HFSD-fed hamsters, the abundance of *Firmicutes*, *Proteobacteria*, and *Actinobacteria* at phylum level

significantly decreased after treated with SCO. An increased *Firmicutes* phylum bacteria alongside decreased *Bacteroidetes* bacteria are likely related to increased food energy absorption and increased low-grade inflammation (Turnbaugh et al., 2006). The ratio of *Bacteroidetes* to *Firmicutes* was significantly correlated with plasma glucose concentrations. In this study, a decrease in bacteria from the *Firmicutes* phylum and an increase in the *Bacteroidetes* bacteria were observed in SCO-treated hamsters. Moreover, SCO could significantly increase *Lactobacillus* and *Bifidobacterium* populations and inhibit the propagation of *Parabacteroides* populations. Numerous studies indicated that diet-induced obesity strongly altered gut microbiota composition by reducing *Bifidobacterium* spp., *Lactobacillus* spp., and *Bacteroides*-related bacteria. In contrast, several *in vivo* studies have demonstrated that diets containing oligosaccharides selectively increased the *Bifidobacteria* and *Lactobacilli* populations. Other studies showed that *Clostridium* species (*Firmicutes* phylum) were negatively correlated to fasting glucose, insulin and plasma triglycerides (Karlsson et al., 2013). *Clostridium* XIVa, which many butyrate-producing species belong to, has been shown to stimulate anti-inflammatory responses in mice, and its abundance is negatively correlated with inflammatory markers in obese subjects (Verdam et al., 2013). SCO, as an oligosaccharide, would be a potential prebiotic to modulate and maintain the microbial community by the metabolites, such as short chain fatty acids fermented by gut microbiota, thus playing a role in relieving liver inflammation and type 2 diabetes. The effects of gut microbiota on the diabetes were intricate, and the relationship between the gut microbiota and the hypoglycaemic, hypolipidaemic, or anti-inflammatory activities of SCO should be investigated in further studies.

Liver is one of the target tissues for insulin action, which results in the glucose uptake and glycogen synthesis in hepatic cells to maintain blood glucose homeostasis. Abundant signalling pathways have been found to be involved in the process of glucose metabolism, of which, the IRS1/PI3K/GLUT4 pathway is highly conserved and regulates glucose uptake in target tissues (Ooms et al., 2009). Insulin-mediated PI3K/Akt-dependent signaling is the major effector of metabolic insulin action and plays a vital role in the regulation of mRNA expression of proteins crucial for gluconeogenesis, glycolysis, and lipid synthesis in the liver (Saltiel and Kahn, 2001). Some key insulin signalling molecules, such as IRS1, PI3K, and GLUT4, are critically involved in glucose metabolism and insulin resistance (Zhu et al., 2013). IRS1, the major substrate proteins generated by phosphorylation of insulin receptor, binds to and activates PI3K. The activation of PI3K is a key step in glucose uptake and insulin-induced glucose transport. AKT (protein kinase B) is accompanied by PI3K activation and further activation GLUT4 by phosphofructokinase to promote the translocation of glucose (Kadowaki et al., 2012). At the cell surface, GLUT4 allows circulating glucose to reduce its concentration gradient by facilitating the diffusion of glucose through muscle and fat cells. Moreover, GLUT4 can join the IRS/PI3K signaling pathway as the insulin-regulated glucose transporter. The JNK signalling, as one of the most important pathways in models of diabetic and obesity, has been shown to contribute to a variety of pathological processes associated with diabetes, obesity, heart disease, and cancer (Kane et al., 2002). It is also more closely related to glycometabolism than lipid metabolism. The above mentioned key genes were collected to investigate whether SCO had the effects on expression of key genes and proteins in the IRS/PI3K and JNK pathways. In our previous study, it was found that after the SCO treatment, the glucose consumption of IR-HepG2 cells were enhanced by 75.3% after treatment with SCO at 200 μg/mL (Yang et al., 2017). In this study, the cell model was used to further investigate the mechanism further. The IRS1/PI3K levels were up-regulated, while JNK1/2 levels were down-regulated after SCO administration. These changes might be beneficial to conduct insulin signal. However, the above results based on *in vitro* cell model were tentative, and only reflect one of the potential active mechanisms of SCO, further validation is needed. Expressions of only few genes were analyzed in present study, and a lack of thorough global gene expression profiles may lead to some bias. Further, the gene and protein expression as well as the protein phosphorylation state should be investigated.

5. Conclusions

Our study showed the hypoglycaemic and hypolipidaemic activities of oligosaccharide from *S. confusum*. SCO possessed great antidiabetic activity in HepG2 cells *in vitro* and in hamsters *in vivo*. It suppressed an increase in glucose level and prevented excessive weight gain, as well as had the potential to stimulate insulin secretion and improve glucose tolerance. The biochemical parameters of blood and histopathology of liver reflected the degree of liver protection provided by SCO against high fat and sucrose diet. Specifically, SCO ameliorated the hepatic insulin resistance by regulating the IRS1/PI3K and JNK signaling pathways. In addition, SCO significantly increased the abundance and diversity of gut microbiota in HFSD-fed hamsters and showed the ability to increase the population of beneficial microbiota and maintain the homeostasis of gut microbiota. Hypoglycaemic and hypolipidaemic activities may relate to the modulation of gut microbiota in hamsters. However, the exact relationship between the gut microbiota and the beneficial activities of SCO should be investigated. Lastly, we recognized that performing additional studies could provide a deeper insight on other relevant physiological processes closely related to those presented here. For instance, SCO might have suffered several chemical modifications but not hydrolyzed and so, derived gut metabolites, either host or microbiota derived, may be more responsible of the observed metabolic effects, particularly regulating insulin signaling pathways. This hypothesis needs further verification by using fluorescent-labeled SCO to track its first-pass metabolism. Overall, SCO has the potential to be a natural source of functional foods and an auxiliary hypoglycaemic or hypolipidaemic drug.

Conflicts of interest

The authors declare no conflict of interest.

Acknowledgments

The project was financially supported by Project of Fuzhou Municipal Bureau of Science and Technology (2018-G-87), Fujian Province Key Laboratory for the Development of Bioactive Material from Marine Algae Grant (2017FZSK05) and Fujian Province Key Laboratory of Quality Science and Processing Technology in Special Starch (FJDF201805). This work was also supported by the project supported by 13th Five-year Plan on Fuzhou Marine Economic Innovation and Development Demonstration Project and Key Laboratory of Marine Biotechnology of Fujian Province.

Transparency document

Transparency document related to this article can be found online at https://doi.org/10.1016/j.fct.2019.110562

Appendix A. Supplementary data

Supplementary data to this article can be found online at https://doi.org/10.1016/j.fct.2019.110562.

References

Barros, F.C.N., Da Silva, D.C., Sombra, V.G., Maciel, J.S., Feitosa, J.P.A., Freitas, A.L.P., De Paula, R.D.M., 2013. Structural characterization of polysaccharide obtained from red seaweed *Gracilaria caudata* (J Agardh). Carbohydr. Polym. 92 (1), 598–603.

Chakrabarti, R., Vikramadithyan, R.K., Mullangi, R., Sharma, V.M., Jagadheshan, H., Rao, Y.N., Sairamb, P., Rajagopalana, R., 2002. Antidiabetic and hypolipidemic activity of *Helicteres isora* in animal models. J. Ethnopharmacol. 81, 343–349.

Cheng, H.N., Neiss, T.G., 2012. Solution NMR spectroscopy of food polysaccharides. Polym. Rev. 52, 81–114.
Ferreira, S.S., Passos, C.P., Madureira, P., Vilanova, M., Coimbra, M.A., 2015. Structure–function relationships of immunostimulatory polysaccharides: a review. Carbohydr. Polym. 132, 378–396.
Garcíajiménez, C., Chocarrocalvo, A., Garcíamartinez, J.M., Castaño, A., Vieja, A.D.L., 2016. From obesity to diabetes and cancer: epidemiological links and role of therapies. Br. J. Canc. 114, 716–722.
Han, Y.R., Ali, M.Y., Woo, M., Jung, H.A., Choi, J.S., 2015. Anti-diabetic and anti-inflammatory potential of the edible brown alga *Hizikia fusiformis*. J. Food Biochem. 39, 417–428.
He, C., Shan, Y., Song, W., 2015. Targeting gut microbiota as a possible therapy for diabetes. Nutr. Res. 35, 361–367.
Holmes, D., 2015. Gut microbiota: antidiabetic drug treatment confounds gut dysbiosis associated with type 2 diabetes mellitus. Nat. Rev. Endocrinol. 12, 61.
Kadowaki, T., Ueki, K., Yamauchi, T., Kubota, N., 2012. Snapshot: insulin signaling pathways. Cell 148 624.e1.
Karlsson, F.H., Tremaroli, V., Nookaew, I., Bergström, G., Behre, C.J., Fagerberg, B., Nielsen, J., Bäckhed, F., 2013. Gut metagenome in European women with normal, impaired and diabetic glucose control. Nature 498, 99–103.
Kane, S., Sano, H., Liu, S.C., Asara, J.M., Lane, W.S., Garner, C.C., Lienhard, G.E., 2002. A method to identify serine kinase substrates. Akt phosphorylates a novel adipocyte protein with a rab gtpase-activating protein (gap) domain. J. Biol. Chem. 277, 22115–22118.
Kumar, S.G., Rahman, M.A., Lee, S.H., Hwang, H.S., Kim, H.A., Yun, J.W., 2009. Plasma proteome analysis for anti-obesity and anti-diabetic potentials of chitosan oligosaccharides in *ob/ob* mice. Proteomics 9, 2149–2162.
Kusminski, C.M., Bickel, P.E., Scherer, P.E., 2006. Targeting adipose tissue in the treatment of obesity-associated diabetes. Nat. Rev. Drug Discov. 15, 639–660.
Li, P.B., Lin, W.L., Wang, Y.G., Peng, W., Cai, X.Y., Su, W.W., 2012. Antidiabetic activities of oligosaccharides of *Ophiopogonis japonicus*, in experimental type 2 diabetic rats. Int. J. Biol. Macromol. 51, 749–755.
Li, R., Zhu, H., Ruan, J., Qian, W., Fang, X., Shi, Z., Li, Y.R., Li, S.T., Shan, G., Kristiansen, K., Li, S.G., Yang, H.M., Wang, J., Wang, J., 2010. *De novo* assembly of human genomes with massively parallel short read sequencing. Genome Res. 20, 265–272.
Liu, L., Heinrich, M., Myers, S., Dworjanyn, S.A., 2012. Towards a better understanding of medicinal uses of the brown seaweed *Sargassum* in traditional Chinese medicine: a phytochemical and pharmacological review. J. Ethnopharmacol. 142, 591–619.
Maciel, J.S., Chaves, L.S., Souza, B.W.S., Souza, B.W.S., Teixeira, D.I.A., Freitas, A.L.P., Feitosa, J.P.A., De Paula, R.C.M., 2018. Structural characterization of cold extracted fraction of soluble sulfated polysaccharide from red seaweed *Gracilaria birdiae*. Carbohydr. Polym. 71, 559–565.
Mazumder, S., Ghosal, P.K., Pujol, C.A., Carlucci, M.J., Damonte, E.B., Ray, B., 2002. Isolation, chemical investigation and antiviral activity of polysaccharides from *Gracilaria corticata* (Gracilariaceae, Rhodophyta). Int. J. Biol. Macromol. 31, 87–95.
Mohammed, K.H., Ahmed, A.D., Han, J., Yin, Y., Kyeongseok, K., Subbroto, K.S., Yang, G.M., Choi, H.Y., Cho, S.G., 2016. Molecular mechanisms of the anti-obesity and anti-diabetic properties of flavonoids. Int. J. Mol. Sci. 17, 569.
Molaei, H., Jahanbin, K., 2017. Structural features of a new water-soluble polysaccharide from the gum exudates of, *Amygdalus scoparia*, Spach (Zedo gum). Carbohydr. Polym. 182, 98–105.
Morgen, C.S., Sørensen, T.I.A., 2014. Obesity: global trends in the prevalence of overweight and obesity. Nat. Rev. Endocrinol. 10, 513–514.
Motshakeri, M., Ebrahimi, M., Goh, Y.M., Othman, H.H., Hairbejo, M., Mohamed, S., 2014. Effects of brown seaweed (*Sargassum polycystum*) extracts on kidney, liver, and pancreas of type 2 diabetic rat model. Evid. Based Compl. Altern. 379–407.
Murphy, E.F., Cotter, P.D., Healy, S., Healy, S., Marques, T.M., O'Sullivan, O., Fouhy, F., Clarke, S.F., O'Toole, P.W., Quigley, E.M., Stanton, C., Ross, P.R., O'Doherty, R.M., Shanahan, F., 2010. Composition and energy harvesting capacity of the gut microbiota: relationship to diet, obesity and time in mouse models. Gut 59, 1635–1642.
Oh, J.H., Kim, J., Lee, Y., 2016. Anti-inflammatory and antidiabetic effects of brown seaweeds in high-fat diet-induced obese mice. Nutr. Res. Pract. 10, 42–48.
Ooms, L.M., Horan, K.A., Rahman, P., Seaton, G., Gurung, R., Kethesparan, D.S., Mitchell, C.A., 2009. The role of the inositol polyphosphate 5-phosphatases in cellular function and human disease. Biochem. J. 419, 29–49.
Saltiel, A.R., Kahn, C.R., 2001. Insulin signalling and the regulation of glucose and lipid metabolism. Nature 414, 799–806.
Shang, Q., Jiang, H., Cai, C., Hao, J., Li, G., Yu, G., 2017. Gut microbiota fermentation of marine polysaccharides and its effects on intestinal ecology: an overview. Carbohydr. Polym. 179, 173–185.
Spyridaki, E.C., Avgoustinaki, P.D., Margioris, A.N., 2016. Obesity, inflammation and cognition. Curr. Opin. Behav. Sci. 9, 169–175.
Turnbaugh, P.J., Ley, R.E., Mahowald, M.A., Magrini, V., Mardis, E.R., Gordon, J.I., 2006. An obesity-associated gut microbiome with increased capacity for energy harvest. Nature 444, 1027–1031.
Verdam, F.J., Fuentes, S., De, J.C., Zoetendal, E.G., Erbil, R., Greve, J.W., Buurman, W.A., Vos, W.M., Rensen, S.S., 2013. Human intestinal microbiota composition is associated with local and systemic inflammation in obesity. Obesity 21, 607–615.
Vinogradov, E., Wasser, S.P., 2005. The structure of a polysaccharide isolated from *Inonotus levis* P. Karst. Mushroom (heterobasidiomycetes). Carbohydr. Res. 340, 2821–2825.
Yang, C.F., Chen, Y.Q., Chen, M.J., Jia, R.B., Liu, B., Zhao, C., 2017. The antidiabetic activity of brown seaweed *Sargassum confusum* polysaccharide hydrolysates in insulin resistance HepG2 cells in vitro. Res. J. Biotechnol. 12, 1–9.
Zhao, C., Gao, L., Wang, C., Liu, B., Yu, J., Zheng, X., 2016. Structural characterization and antiviral activity of a novel heteropolysaccharide isolated from *Grifola frondosa*, against enterovirus 71. Carbohydr. Polym. 144, 382–389.
Zhao, C., Wu, Y.J., Liu, X.Y., Liu, B., Cao, H., Yu, H., Sarker, S.D., Nahar, L., Xiao, J.B., 2017. Functional properties, structural studies and chemo-enzymatic synthesis of oligosaccharides. Trends Food Sci. Technol. 66, 135–145.
Zhao, C., Yang, C.F., Liu, B., Lin, L., Sarker, S.D., Nahar, L., Yu, H., Cao, H., Xiao, J.B., 2018. Bioactive compounds from marine macroalgae and their hypoglycemic benefits. Trends Food Sci. Technol. 72, 1–12.
Zhao, C., Yang, C.F., Wai, S.T.C., Zhang, Y.B., Portillo, M.Y., Paoli, P., Wu, Y.J., Cheang, W.S., Liu, B., Carpéné, C., Xiao, J.B., Cao, H., 2019. Regulation of glucose metabolism by bioactive phytochemicals for the management of type 2 diabetes mellitus. Crit. Rev. Food Sci. 59, 830–847.
Zhu, Y., Pereira, R.O., O'Neill, B.T., Riehle, C., Ilkun, O., Wende, A.R., Rawlings, T.A., Zhang, Y.C., Zhang, Q., Klip, A., Shiojima, I., Walsh, K., Abel, E.D., 2013. Cardiac PI3K-Akt impairs insulin-stimulated glucose uptake independent of mTORC1 and GLUT4 translocation. Mol. Endocrinol. 27, 172–184.